Applied Energy 147 (2015) 161–175

Contents lists available at ScienceDirect

Applied Energy

journal homepage: www.elsevier.com/locate/apenergy

Characterization of viscous biofuel sprays using digital imaging in the near field region

J.L.H.P. Sallevelt *, A.K. Pozarlik, G. Brem

University of Twente, Department of Energy Technology, Drienerlolaan 5, 7522 NB Enschede, The Netherlands

HIGHLIGHTS

- Biodiesel, vegetable oil and glycerin sprays have been studied using PDIA.
- The study is focused on the effect of fuel viscosity on the spray characteristics.
- Viscosity has a strong effect on the breakup length in pressure-swirl atomization.
- The results are compared to combustion experiments with a micro gas turbine.
- The penetration depth of ligaments can be a critical factor in burning viscous fuel.

ARTICLE INFO

Article history:
Received 18 July 2014
Received in revised form 29 January 2015
Accepted 30 January 2015

Keywords:
Gas turbine
Atomization
PDIA
Shadowgraphy
Biofuels

ABSTRACT

The atomization of biodiesel, vegetable oil and glycerin has been studied in an atmospheric spray rig by using digital imaging (PDIA). Images of the spray were captured in the near field, just 18 mm downstream of the atomizer, and processed to automatically determine the size of both ligaments and droplets. The effect of the spray structure in this region is of major interest for the combustion of biofuels in gas turbines. The sprays were produced by a pressure-swirl atomizer that originates from the multifuel micro gas turbine (MMGT) setup. Various injection conditions have been tested to investigate the influence of viscosity on the spray characteristics and to assess the overall performance of the atomizer. The spray measurements have been compared to combustion experiments with biodiesel and vegetable oil in the micro gas turbine at similar injection conditions. The results show that the primary breakup process rapidly deteriorates when the viscosity is increased. A higher viscosity increases the breakup length, which becomes visible at the measurement location in the form of ligaments. This effect leads to an unacceptable spray quality once the viscosity slightly exceeds the typical range for conventional gas turbine fuels. The SMD in the investigated spray region was not significantly affected by viscosity, but mainly influenced by injection pressure. The data furthermore indicate an increase in SMD with surface tension. It was found that the penetration depth of ligaments can have major impact on the combustion process, and that the droplet size is not always the critical factor responsible for efficient combustion. The measured delay in primary breakup at increased viscosity shows that pressure-swirl atomization is unsuitable for the application of pure pyrolysis oil in an unmodified gas turbine engine.

1. Introduction

To increase the share of renewables and to reduce CO_2 emissions in future power generation, a considerable amount of research has been conducted on fuels derived from biomass sources. One of the biofuels developed in the last few decades is pyrolysis oil, also known as bio-oil, biocrude or pyrolysis liquid. Pyrolysis oil can be produced from a variety of forest and agricultural biomass waste materials [1] via thermochemical decomposition in absence of oxygen. The dark brown, combustible liquid that results from this process with a yield of 65–75 wt.% is considered as a promising alternative for fossil fuels in industrial applications. However, the presence of a large amount of oxygenated compounds gives pyrolysis oil markedly different properties compared to conventional petroleum-derived fuels. The difference in fuel properties has led to a number of technical hurdles that need to be addressed before application in combustion devices can be successful on the long term.

An interesting possibility is the use of pyrolysis oil in gas turbine engines. Gas turbines are relatively fuel-flexible and are capable of generating power on both large and small scales, suiting the

* Corresponding author.
E-mail address: j.l.h.p.sallevelt@utwente.nl (J.L.H.P. Sallevelt).

http://dx.doi.org/10.1016/j.apenergy.2015.01.128
0306-2619/

demands of the future energy system. Pyrolysis oil combustion in gas turbines has therefore been subject of a few experimental studies in the past years [2–8]. These studies, conducted in both scientific and industrial test rigs, have shown that the use of pure pyrolysis oil often leads to major problems. Reported issues include high CO emissions, flame instability, fuel deposits in the hot section and unburned particles in the exhaust gas.

The poor burning characteristics of pyrolysis oil are related to its low volatility, low heating value and limited stability, but can also be attributed to the fuel spray quality. Pyrolysis oil has a high viscosity with respect to the conventional fuels, which causes the atomization process to be less effective [9]. Preheating the oil in order to reduce the viscosity to an acceptable level is only allowed to a limited extent, because certain reactive compounds tend to polymerize at elevated temperatures. Whereas the atomization of pyrolysis oil can be problematic for this reason, it is essential to deliver very fine sprays to cope with the adverse combustion properties of this biofuel. Improving the atomization is not only required to restrict the evaporation time, but can also largely prevent the formation of carbon-rich particles which are sometimes seen as sparks during combustion tests. Previous studies have shown that the amount of solid residue after evaporation decreases with the drop size, since polymerization reactions are suppressed at high heating rates [10,11].

For these reasons, it is important to measure and compare the quality of sprays under different conditions. Information on the influence of fuel properties helps to further define biofuel specifications and atomization requirements for combustion applications. Spray measurements are furthermore essential for understanding some of the phenomena that occur during test campaigns with various viscous biofuels, i.e. to separate the effects of spray charactistics from those of chemical kinetics.

The literature concerning the atomization of pyrolysis oil or other viscous fuels for gas turbine applications is scarce. Only few studies on this topic have been found, which consider a variety of atomizers, liquids, test conditions and sample locations. Detailed information on the spray in the near field region is not often reported in these studies, presumably due to measurement difficulties. However, the spray characteristics close to the atomizer are of special interest for evaporation and mixing, and besides most relevant as input data for spray combustion models in CFD.

Krumdieck and Daily [12] were among the first researchers to study the atomization of pyrolysis oil. They tested internally and externally mixed air-assist atomizers for use in spray combustion experiments with this biofuel. The authors concluded that the internally mixed atomizer performed much better, but did not describe the spray quality in terms of droplet size.

López Juste and Salvá Monfort [2] studied the general appearance of a pyrolysis oil spray produced by a pressure-swirl atomizer in preparation for combustion tests. To obtain a viscosity below 10 cP, the pyrolysis oil was preheated to 115 °C. They found that the spray angle decreased from the standard value of 60° for diesel to only 20° for pyrolysis oil. The cause of this remarkable change was not identified. Since the researchers wanted to avoid any major modifications to their injection system, the combustion tests were carried out using a mixture of pyrolysis oil and ethanol to lower the viscosity. Figures defining the spray quality were not discussed.

Significant work on pyrolysis oil atomization has been done by Garcìa-Pèrez et al. [13]. Their study includes drop size measurements in sprays of pyrolysis oil (at 80 °C), No. 2 diesel (at 25 and 40 °C) and water (at 25, 60 and 80 °C). The sprays were produced by two different Delavan pressure-swirl atomizers (type A and W) at varying injection pressures. Droplet sizes between 2 and 197 μm were measured 50 mm downstream of the atomizer using Malvern Mastersizer equipment, which is based on laser diffraction technology. Within the tested range of injection pressures, the Sauter mean diameter (SMD) of the pyrolysis oil sprays was 45–75 μm for atomizer type A, and 35–70 μm for atomizer type W. These values were typically 10–20 μm higher than those measured in the diesel and water sprays. The difference was attributed to the relatively high viscosity of the pyrolysis oil, which was still 17 cP despite preheating to 80 °C.

Atomization studies related to other viscous biofuels than pyrolysis oil can provide useful insights as well. Crayford et al. [14] investigated the pressure-swirl atomization of a bio-oil derived from the food industry. Details about the viscosity of the bio-oil are not given, but a temperature of 27.5 °C was indicated as the melting point. The researchers used phase Doppler anemometry (PDA) to record the droplet size and velocity simultaneously at a specified point, while backlight photography was employed for providing information on the general spray structure. The global SMD of the full cone bio-oil spray, derived from local measurements at 6 axial and 9 radial positions, decreased from 59 to 55 μm when preheating the fuel from 60 to 80 °C. At 80 °C, the global SMD and structure of the bio-oil spray and the benchmark gas-oil spray were similar. However, the authors underline that characterization of an entire spray using a single drop diameter is problematic. Close to the atomizer, 25 mm downstream, a preheat temperature of only 70 °C would be necessary to match the SMD measured in the gas-oil case.

Panchasara and Agrawal [15] examined straight vegetable oil (VO) sprays produced by an airblast atomizer at different oil temperatures and air-to-liquid ratios (ALR). Laser sheet visualization was used to capture spray images for qualitative analysis. Quantitative, pointwise measurements of droplet diameters and gas phase velocities in the full cone were performed with a phase Doppler particle analyzer (PDPA) system. It was found that an increase in oil temperature and ALR both improve the atomization, especially in the outer region of the spray. However, with a maximum SMD of only 60 μm for a VO viscosity of 28 cP, good atomization was achieved even at low oil temperature and low ALR. In the near field, 20 mm downstream, the SMDs were below 42 μm at all conditions.

Recently, interesting results have been presented on the atomization of viscous fuels using a novel method referred to as 'flow-blurring' [16–18]. In this concept, air penetrates the fuel flow in a region close to the orifice to create a turbulent two-phase mixture. The air bubbles contained in the fuel rapidly expand when exiting the nozzle, thereby disintegrating the liquid structure. This technique has been shown to deliver superior atomization performance compared to conventional airblast atomization methods and is suggested to have an advantage over effervescent atomization regarding the flow stability inside the atomizer. Droplet size measurements using PDPA in reacting glycerol sprays and in non-reacting vegetable oil and diesel sprays produced by a flow-blurring atomizer have been reported by Simmons and Agrawal [18,19]. Without preheating the liquids, they obtained SMDs of typically 25–40 μm in the glycerol spray (100 mm downstream) and 35–55 μm in the near field of the vegetable oil spray (20 mm downstream). Such SMDs are exceptionally low, considering the viscosities of respectively 930 and 50 cP. The flow-blurring atomizer is still in the research phase and not (commonly) used in practical combustion applications yet.

In this work, the effect of viscosity on spray quality has been assessed by using an economically attractive high-resolution particle imaging technique (PDIA). Sprays of three different liquids were visualized at varying injection conditions in the region near the atomizer to investigate the primary atomization process. The size of the droplets captured on the images was then determined via automated analysis. Also the effect of ligaments in the proximity of the atomizer was taken into account, showing the significance

of a proper primary breakup process. The investigated sprays were produced by the pressure-swirl atomizer from the multifuel micro gas turbine (MMGT) setup at the University of Twente. The droplet size data resulting from this study can therefore be compared with exhaust gas emissions measured in combustion experiments [20].

2. Research method

The droplet size measurements in the present study have been performed using a non-intrusive optical technique referred to as particle/droplet image analysis (PDIA) [21]. In this method, the spray is first visualized by capturing shadow images of the droplets. The spray images are then analyzed on a computer using a Matlab script for automatic recognition and sizing of the droplets.

Among the methods available for sizing droplets, direct imaging has until recently been an uncommon technique for the characterization of sprays used in combustion applications. Limitations in resolution and sensitivity made photography unreliable or too costly for sizing the small droplets in the range 10–100 μm, which is typical for fuel sprays. Thanks to great progress in digital imaging technology, however, PDIA has proven to be a robust, accurate and cost-effective tool for research on fuel atomization [21,22]. The method has besides an important advantage over other techniques, such as PDA, since it delivers a visual impression of the spray structure. This allows for detecting liquid fragments of any shape and gives good insight into the breakup process as shown in several studies [23–29].

In this section, the experimental setup that was developed for capturing high quality images of the spray will be explained first. Subsequently, details are given about the methods used for analyzing the images to evaluate the spray quality.

2.1. The spray imaging setup

The spray imaging setup has been designed to visualize individual droplets in a spray at different pressures and temperatures. Following the principle of shadowgraphy, a downward spray is exposed to a light source on one side, providing background illumination for a camera that is located on the opposite side. As the droplets reflect or deflect the majority of the incident backlight, they are seen as dark spots on the image when crossing an imaginary measurement volume defined by the position and optical characteristics of the camera. This configuration is schematically illustrated in the setup overview shown in Fig. 1. The position of the light source in the setup is fixed, while the camera position can be adjusted electronically to shift the focal plane towards the desired location in the spray. The location of the camera is horizontally and vertically measured with micrometer accuracy using a linear encoder system.

A frequency-doubled Nd:YAG laser serves as the light source for the measurements. The laser emits light with a wavelength of 532 nm, a pulse duration of 6 ns and a maximum pulse energy of 1 J. These pulses were short enough to avoid any motion blur and sufficiently intense to obtain good contrast in the images. However, direct use of the laser spot results in a highly disturbing speckle pattern due to mutual interference of the single-frequency light waves. Hence, after entering the spray chamber, the laser beam penetrates a glass flow cell with a fluorescent dye solution. The light emitted by the dye covers a wider spectral range and provides high quality, uniform illumination of the image background. A ground glass diffuser is placed just in front of the flow cell to obtain a more uniform laser spot for excitation of the dye.

The droplets in the spray are captured using a digital camera (Nikon D5200) with a resolution of 6000 × 4000 pixels. The images on the sensor are formed by a micro lens (Tamron 180 mm F3.5

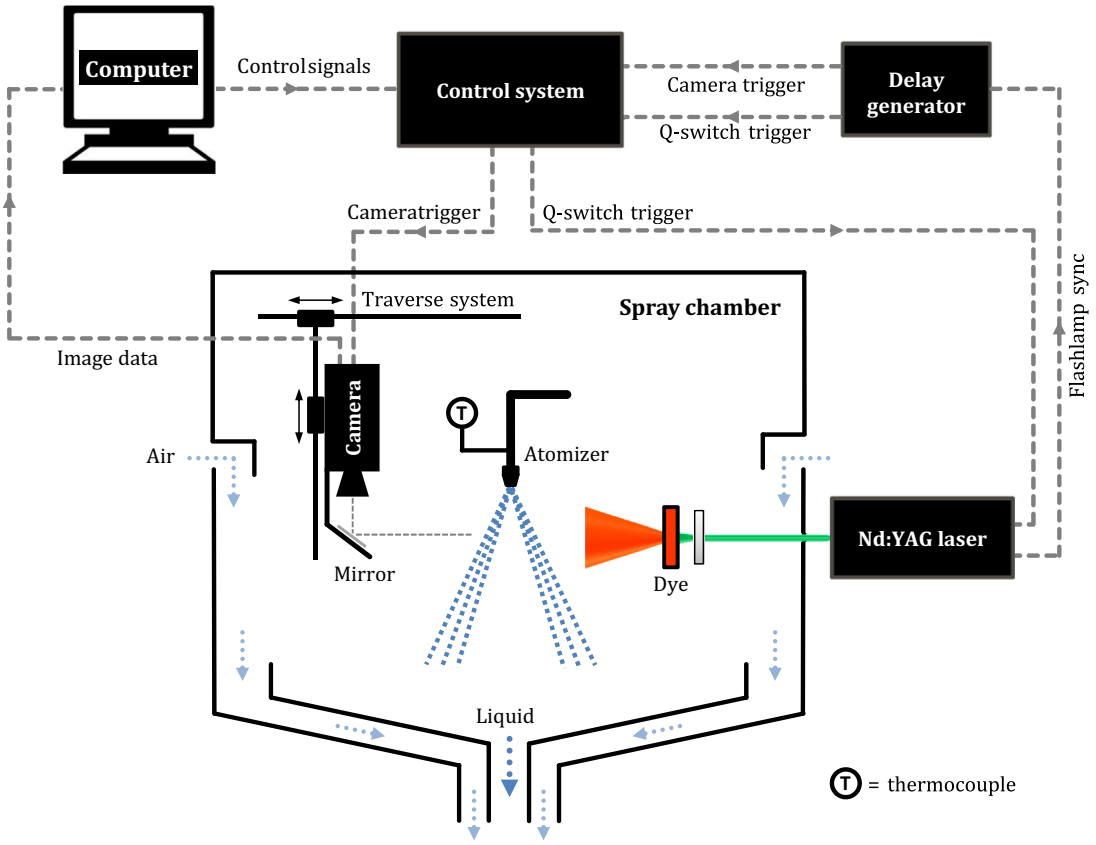

Fig. 1. Schematic overview of the spray imaging setup.

Macro 1:1) and a teleconverter (Kenko DG MC 3X PRO300), which together achieve a maximum reproduction ratio of 3:1. This combination resulted in an optical system with sufficient magnification and resolution to capture the droplets at a suitable focal distance. All three components are mounted vertically in a box to protect the system against the spray. Images are captured through a glass window in the bottom of the protection box and via a silver-coated mirror underneath. The camera is remotely controlled and sends the images directly to the computer.

The timing of the laser Q-switch and the camera shutter is managed by a delay generator. By activating the triggering scheme programmed in the delay generator, the image capturing is performed automatically with a total cycle time of 2 s per image.

An external fuel supply system is used to control the liquid flow. This system is able to supply liquid to the atomizer at pressures up to 60 bar and temperatures up to 100 °C. The liquid temperature is measured close to the atomizer using a K-type thermocouple in the flow.

In order to prevent accumulation of mist inside the setup, the air inside the spray chamber is ventilated by using a centrifugal air extractor. The air inlets are located in the side walls to minimize interactions between the air flow and the spray.

2.2. Digital image analysis

The images captured in the experimental setup are automatically analyzed using a Matlab script. The script is developed to recognize spherical as well as non-spherical liquid objects in the image and rejects any objects of which the size cannot be determined accurately. The output data contain the relevant geometric properties of all accepted objects, which are used to calculate the overall spray characteristics.

Firstly, the quality of the raw image data is assessed by checking the intensity of the background illumination. Since the object recognition method is based on contrast, the results from the script are rather sensitive to variations in background intensity. Images with insufficient overall contrast are therefore removed from the raw data set. Very few images were rejected, however, as the exposure was generally constant during the measurements.

The remaining images are then analyzed by the script, following the procedure that is schematically shown in Fig. 2. The procedure starts by converting the raw RGB image to grayscale and enhancing the contrast. The enhanced image is then reduced to a binary image in black-and-white (B/W) using a certain threshold value. The binary image is the input for the Canny edge detection [30], of which the result is improved by a cleanup process. Edges with single-pixel gaps (equivalent to 1.47 μm) are closed, whereas edges with larger gaps are discarded. Closed edges mark the contours of objects in the image.

After identifying the objects, their pixel regions are used to determine the relevant geometric properties. Here, the effective diameter is derived from the surface area to increase the linear accuracy. Objects that are smaller than the chosen size threshold are removed, because the sizing method becomes inaccurate if an object contains only a few pixels.

The objects are then classified as either droplets or ligaments based on the roundness parameter $4\pi A_c/p^2$, where A_c is the cross section area and p is the perimeter. This parameter is unity if the

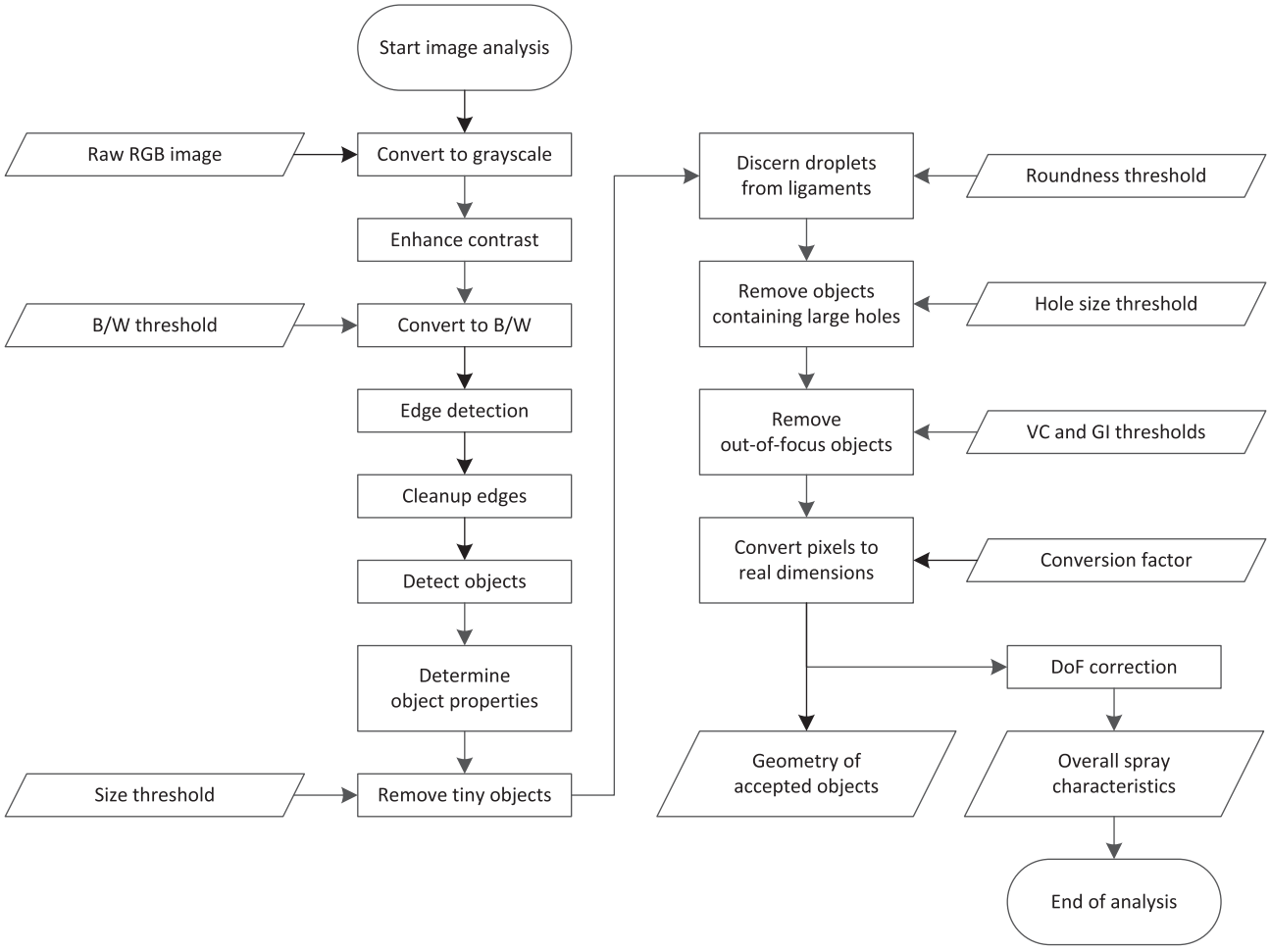

Fig. 2. Process flow diagram of the image analysis script.

Fig. 3. Circles on the reticle as captured in the setup.

cross section of the object is perfectly circular, and goes towards zero if the shape deviates from a circle. In this study, objects are marked as non-spherical if the parameter is below the threshold of 0.25. Droplets or ligaments containing considerable cavities are removed after hole detection. Holes in an object lead to errors, since the objects are identified on basis of the outer edge and cavities would be considered as part of the liquid phase.

Subsequently, it is essential to determine if the detected objects are in focus. The sizing of objects that are located partly or entirely out of the measurement volume is unreliable due to a lack of contrast with the background. The out-of-focus detection in the script is based on the approach described by Lee and Kim [31], who propose to use a combination of two parameters. The first is the gradient intensity (GI), evaluating the average normal gradient at the object boundary. The second parameter is the value of contrast (VC), which is defined as the normalized maximum contrast between the object and the background. The VC can be more effective for testing small objects. The droplet and ligaments are considered in focus only if both the GI and VC criteria are satisfied.

Converting the geometric object properties from pixels to micrometers gives the final output data for the individual droplets and ligaments. These data contain the surface area, the perimeter and, in case of droplets, the effective diameter. However, when the overall spray quality is evaluated by calculating a mean diameter, the droplet data needs to be corrected for differences in the depth of field. The depth of field (DoF) of the optical system is here defined as the depth of the imaginary measurement volume around the focal plane, in which objects are photographed acceptably sharp for measuring their size with good accuracy. This optical property depends on the size of the object to be captured, see Fig. A.23. Similar trends were found by Lee and Kim [31] and by Castanet et al. [29]. Since the depth of field starts to decrease when the object size falls below a certain limit, the method is naturally biased towards large droplets and ligaments. The depth of field correction that has been applied to compensate for this effect is described in Section 3.2.

In the analysis procedure described above, certain input parameters need to be defined that have influence on the final result. As can be seen in Fig. 2, the script uses several threshold values as well as a conversion factor between pixels and micrometers. Furthermore, a depth of field correction is used to obtain a more realistic result for the spray quality. To minimize the measurement error and optimize the setup's capabilities, the most influential input values have been defined by measuring the system characteristics and by calibration. The results from these activities are described in Section 3 and Appendix A.

3. Optimization of the method

The characteristics of the optical arrangement are mainly expressed by the focus distance, field of view, reproduction ratio, exposure and depth of field. These properties are largely determined by the hardware, but are also influenced by the zoom and aperture setting. A parameter study was therefore performed to optimize the system settings for the droplet size measurements. The optical characteristics are furthermore required to define and optimize the input values for the image analysis script as described in Section 2.2.

3.1. Optimization procedure

To measure the reproduction ratio and the depth of field at different settings, a Patterson globe reticle [32] was used as a reference. The 10 circles with different diameters that are printed on the glass surface cover the size range representative for the droplets to be measured. Fig. 3 shows the circles as captured by the camera in the spray imaging setup. Here, the circle diameter decreases from 450 μm on the left to 18 μm on the right.

The reproduction ratio is found by capturing the reticle in the focal plane. The circle diameters in terms of pixels as measured using the analysis script are then compared to their real sizes. This ratio directly gives the pixel-to-micron conversion factor, which is equivalent to the reproduction ratio. Once the conversion factor is known, the depth of field can be determined by photographing the circles at varying distance from the focal plane until they appear completely blurred. The threshold values in the script that govern the in-focus criteria are then adapted such that the measurement error is acceptable for each size (see Fig. 4). Since changing the threshold values also affects the conversion factor, these parameters have been optimized in an iterative process.

3.2. System characteristics and accuracy

On basis of the results from the parameter study, the zoom setting was chosen as a trade-off between focus distance, reproduction ratio and depth of field. The aperture setting followed from balancing the exposure and depth of field. For this optimized configuration, the conversion factor is measured to be 1.47 μm/px. The associated field of view is about 8.8 × 5.9 mm as a consequence of the sensor resolution.

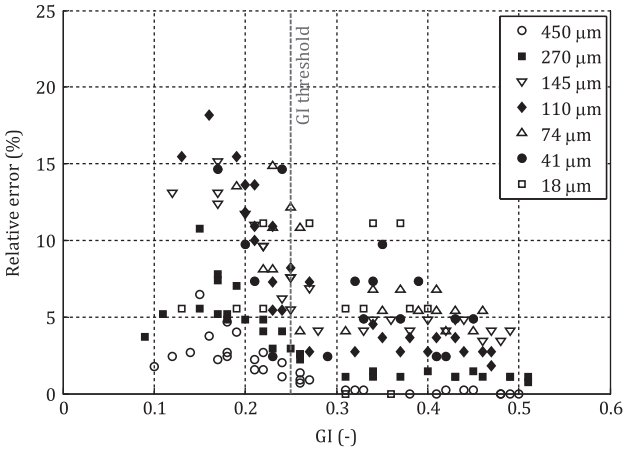

Fig. 4. Relative measurement error as function of the GI.

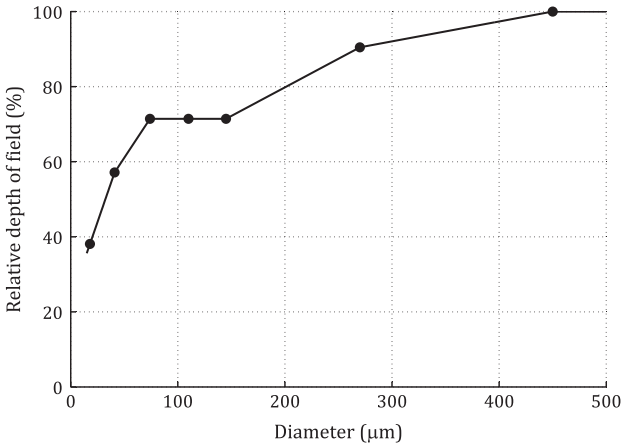

Fig. 5. Relative depth of field as function of the object size.

The input parameters of the analysis script were adjusted such that the measurement error is restricted to an acceptable level. From the results of the depth of field analysis given in Appendix A, it can be concluded that the GI parameter is effective for controlling the error by rejecting the out-of-focus objects of any size. The percentual measurement error relative to the circle size is shown as function of the GI in Fig. 4. By choosing a GI of 0.25, as indicated in the figure, the maximum relative error in the investigated size range from 18 to 450 μm is kept under 12% of the object diameter.

The VC has a nearly constant value of 1 for all circles larger than 40 μm due to the fact that even blurry objects have a very dark area in the center. Therefore, the VC is generally unsuitable as a selection criterium in this case. A useful relation between the VC and the distance from the focal plane is only observed for the smallest circle of 18 μm, but also for this size the GI is found to be more strict so that the VC is completely overridden.

The graphs shown in Appendix A also illustrate that the depth of field increases with the object size. According to Fig. A.21, the depth of field ranges from 400 μm for the 18 μm circle to 1050 μm for the 450 μm circle when the GI is set to 0.25. The markers in Fig. 5 indicate the depths of field measured for the sample diameters considered in the analysis, relative to the depth of field for the largest circle (450 μm). To construct a curve over the entire range, the markers are connected using linear segments. The depth of field correction applied in the script is performed by dividing the number of detected droplets of a certain size by the corresponding value prescribed by Fig. 5. This way, the relative depth of field is virtually restored to 100% for all object sizes.

An effective object diameter of 15 μm is chosen as the lower detection limit of the method. This diameter, represented by 10 pixels on the image sensor, is adopted as the size threshold in the analysis script (see Fig. 2).

4. Test conditions

4.1. Atomizer specification

The sprays in the atomization tests were produced by the pressure-swirl atomizer that originates from the multifuel micro gas turbine (MMGT) setup at the University of Twente. A drawing of this atomizer is given in Fig. 6. The atomizer produces a hollow cone spray with an angle of 90 to 100° and is characterized by a flow number of $41 \cdot 10^{-8}$ m^2. The flow number was experimentally determined and can be used to accurately describe the mass flow rate through the atomizer via the following relation [9]:

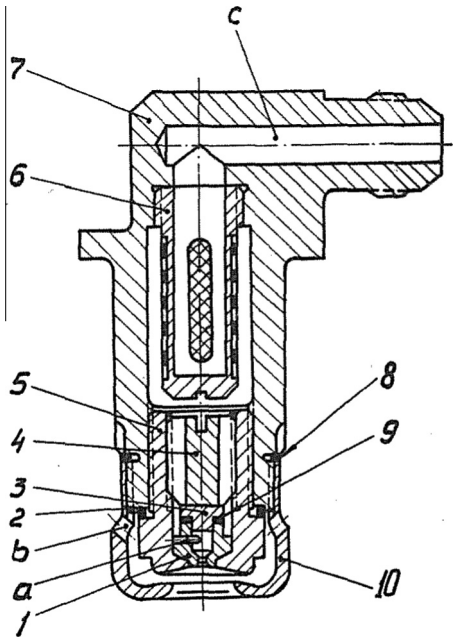

Fig. 6. Drawing of the tested pressure-swirl atomizer: 1 – swirl chamber housing, 2 – gasket, 3 – pressure piece, 4 – nozzle screw, 5 – nozzle body, 6 – filter, 7 – housing, 8 – gasket, 9 – gasket, 10 – nozzle cap, a – swirl chamber inlet, b – cooling air inlet, c – fuel inlet. Reproduced from [33].

$$\dot{m} = \mathrm{FN}\sqrt{\rho_l \Delta p} \tag{1}$$

where FN is the flow number, ρ_l is the liquid density and Δp is the applied pressure difference.

4.2. Properties of the tested liquids

The spray characteristics have been studied for three different liquids: biodiesel (BD), vegetable oil (VO) and glycerin (GL). These liquids have been selected to investigate the effect of mainly viscosity on the average spray quality. Together with the density and surface tension of the liquid, the viscosity is seen as one of the relevant properties in pressure atomization [9]. Since the density and surface tension are much weaker functions of temperature, preheating primarily influences the viscosity of the liquids. This is illustrated by Table 1, where the properties of interest are given for the three liquids at the minimum and maximum temperature used in the experiments.

The properties of biodiesel at 60 °C are equal to those of No. 2 diesel at room temperature. The spray characteristics for biodiesel at this temperature should therefore be representative for operation at standard diesel fuel. The liquid referred to as vegetable oil here is actually a mixture of straight vegetable oils that is characterized by a high viscosity. The density of this oil mixture is slightly higher compared to biodiesel, whereas the surface tension is nearly the same within the respective temperature ranges. Both these

Table 1
Variation in biodiesel, vegetable oil and glycerin properties over the tested temperature ranges. Viscosities were measured, densities and surface tensions were obtained from [34–36].

Property	Unit	Biodiesel		Vegetable oil		Glycerin	
	°C	20	60	50	100	60	100
Density	kg/L	0.87	0.84	0.90	0.87	1.18	1.15
Surface tension	mN/m	32	28	31	28	62	58
Viscosity	cP	6.3	2.3	17.9	4.9	17.0	4.8

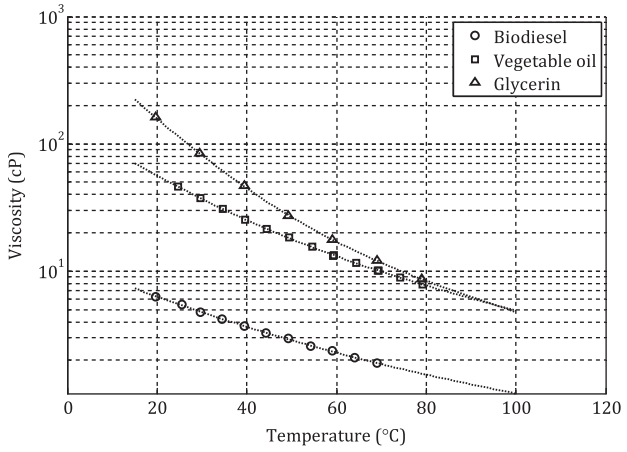

Fig. 7. Measured viscosity of the three tested liquids as function of temperature.

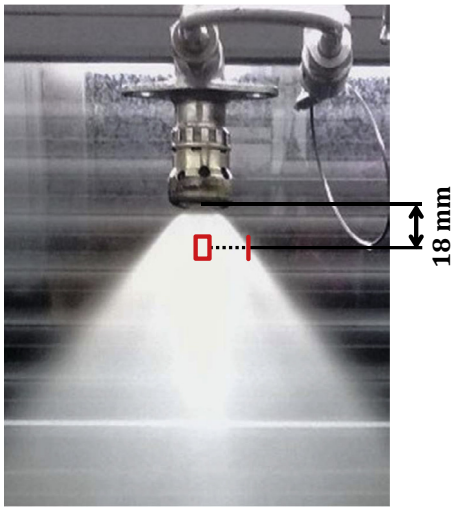

Fig. 8. Impression of the size and location of the focal plane in the spray.

fuels were recently tested in the MMGT setup to measure the effect of fuel viscosity on the exhaust gas emissions [20]. The spray quality measured in the present study can therefore be compared to emission data obtained from the combustion tests.

The glycerin is a 77 wt.% glycerol/water mixture, which is chosen as a test liquid to investigate the influence of viscosity when also the density and surface tension are considerably higher than those of the standard fuels. Testing with a high surface tension is relevant because values up to 40 mN/m have been measured for pyrolysis oil at room temperature [37], whereas the typical value for diesel is 28 mN/m. The surface tension for the glycerin is even higher than for pyrolysis oil, however, so that the effect of this property will be exaggerated. The density of the glycerin is in good agreement with that of pyrolysis oil.

Since the study is focused mainly on the influence of viscosity in relation to atomization quality, this fluid property was measured as function of temperature using a Brookfield DV-II + Pro viscometer. The results are shown in Fig. 7, where regression curves indicate the viscosity outside of the measurement range.

4.3. Operating conditions

An overview of the atomizer operating conditions is shown in Table 2. All images have been captured 18 mm downstream of the atomizer, see Fig. 8. This sample location corresponds to the height where the primary breakup process is just completed in the biodiesel spray at 10 bar and 20 °C. The optical system was configured as defined in the optimization procedure. However, the ISO value was adjusted to compensate for a reduction in camera exposure at higher injection pressures, presumably caused by a higher spray density or a slight increase in spray cone angle.

The images are uncorrelated snapshots of a quasi-steady spray. Since it is a matter of coincidence which part of the spray is present in the measurement volume, a sufficient number of images are required to determine the average spray characteristic at the sample location. Preliminary image data has shown that the mean droplet size indeed fluctuates for each image but converges to a constant value by including more images in the dataset. To ensure a converged result, 80 to 100 images were captured at each injection condition. As an example, the convergence of the SMD for three different sprays is given in Appendix B.

Table 2
Overview of the atomizer operating conditions.

Liquid	Pressures (bar)	Temperatures (°C)
Biodiesel	10, 20, 30	20, 30, 40, 60
Vegetable oil	10, 20, 30	50, 60, 70, 80, 90, 100
Glycerin	10, 20, 30	60, 70, 80, 90, 100

5. Results and discussion

Objects detected in the image analysis procedure are marked as either spherical or non-spherical. This feature allows to evaluate the atomization quality for combustion applications on basis of droplets as well as ligaments. Information on both types of objects is reported by expressing the results in terms of three different parameters that are used as spray quality indicators: the normalized ligament area (NLA), the mean ligament size (MLS) and the Sauter mean diameter (SMD).

The influence of pressure and temperature is shown by discussing the results for biodiesel, vegetable oil and glycerin sprays sequentially. Figure axes have been fixed for convenient comparison of results for the different liquids. The experimental data are subsequently compared to the combustion performance as measured in the MMGT setup. Implications for pyrolysis oil combustion in the MMGT setup will be considered at the end of this section.

5.1. Spray quality indicators

In pressure-swirl atomization, the liquid leaves the nozzle orifice in the form of a thin, conical sheet. Instabilities in the liquid cause the sheet to disintegrate into elongated structures or ligaments, which then break up further to form droplets [38]. This process is usually referred to as primary breakup. The droplets may then split up further due to interactions with its surroundings during secondary breakup. Images containing ligaments thus show that the primary breakup process was incomplete or that secondary breakup of big drops is occurring at the measurement location. In this study, the capturing of ligaments formed during primary breakup is promoted by measuring close to the atomizer.

The content of non-spherical objects in the measurement data has been quantified by calculating the normalized ligament area (NLA). This parameter is defined as the total area represented by ligaments, normalized with the total area of both ligaments and droplets as measured in the images:

$$\mathrm{NLA} = \frac{\sum A_{\mathrm{c,lig}}}{\sum A_{\mathrm{c,lig}} + \sum A_{\mathrm{c,drop}}} \tag{2}$$

where A_c refers to the cross-sectional area.

The NLA can be used as an indicator for primary breakup, though also secondary breakup has influence on its value. In the latter case, however, the elongated shape is not representing a ligament directly originating from the liquid film, but defining the contours of a heavily distorted droplet. Such objects are typically smaller than ligaments and are beneficial for the spray quality due to their higher surface-to-volume ratio. They are besides likely to break up into even smaller droplets in the next moment, which evidently leads to faster evaporation. Poor atomization is hence indicated only by the considerably larger ligaments formed during primary breakup. Therefore, in case the NLA of a spray is substantial, it is relevant to determine the size of the ligaments as well. To this end, an additional parameter expressing the mean ligament size (MLS) is defined as the total ligament area divided by the total number of ligaments:

$$\mathrm{MLS} = \frac{\sum A_{c,\mathrm{lig}}}{N_{\mathrm{lig}}} \tag{3}$$

The NLA and MLS parameters together give essential information about the atomizer performance at certain injection conditions. It must be noted, however, that flawless detection of ligament boundaries is more challenging than resolving droplet boundaries. The most complex shapes are therefore not always properly recognized, so that some of the ligaments can be missing in the data set. Still, despite this deficiency, the ligament data is useful for indicating the trends.

In addition to the NLA and MLS, the Sauter mean diameter (SMD or D_{32}) is used as a third indicator for evaluating the atomizer performance. The SMD is a suitable measure for the mean droplet size when evaporation is important as it compares the total spray volume to the total surface area. Its definition is given by Eq. (4), where D_{drop} is the calculated effective diameter of the droplet based on its area. The non-spherical objects are not taken into account here, because their volumetric shape is rather arbitrary.

$$\mathrm{SMD} = \frac{\sum D_{\mathrm{drop}}^3}{\sum D_{\mathrm{drop}}^2} \tag{4}$$

5.2. Results for biodiesel

Fig. 9 shows the NLA as function of pressure for the biodiesel sprays at 20 to 60 °C. Considering the low values, the primary breakup process can be assumed to be complete at all conditions. The graph also shows that the temperature has no significant effect. Apparently, the changes in biodiesel properties over the temperature range are relatively small in relation to atomization.

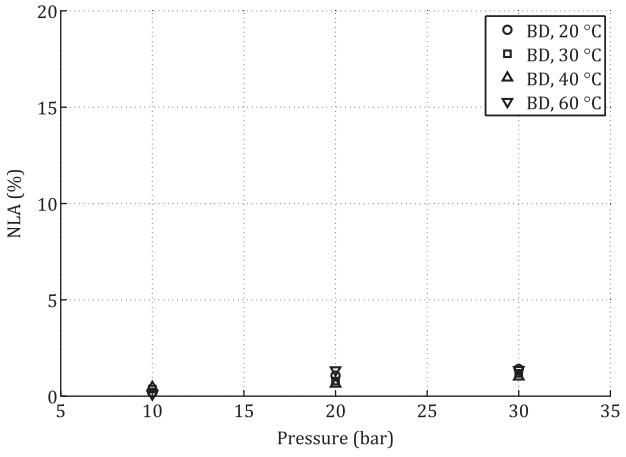

Fig. 9. Normalized ligament area as function of pressure for biodiesel.

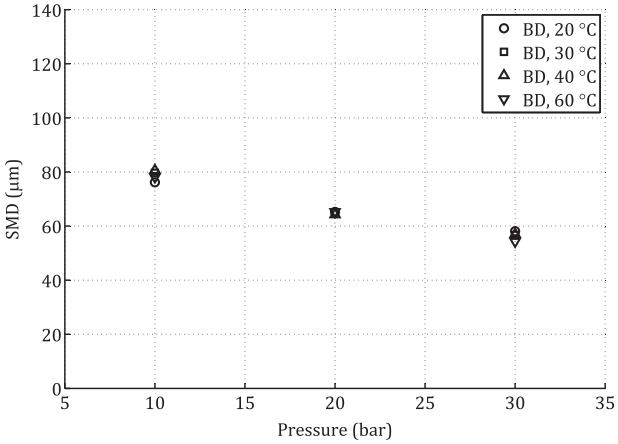

Fig. 10. SMD as function of pressure for biodiesel.

By raising the pressure, however, the NLA is observed to slightly increase. This trend can be mainly attributed to secondary breakup of large droplets. A larger pressure drop over the orifice results in stronger instabilities propagating in the liquid, which can be dominant over the surface tension forces that tend to restore the spherical shape. In such cases, the liquid elements are detected as ligaments instead of droplets. The secondary breakup process leads to a better spray quality, since the volume-to-surface ratio of a stretched droplet is more favorable and some of the large droplets will split up. Another possible explanation is the higher exit velocity at the atomizer orifice. Since the measurement location is fixed in space, the available breakup time becomes shorter when increasing the pressure and breakup might have not taken place yet for a small part of the ligaments. Given the fact that the MLS is not increasing with pressure, however, this effect is most likely not significant here.

The SMD as function of pressure is reported in Fig. 10 for the different temperatures. Increasing the pressure from 10 to 30 bar leads to a considerable reduction in SMD, roughly from 80 down to 60 µm. Again, no clear effect of temperature is observed. It can therefore be concluded that the spray quality at the sample location is insensitive to variations in viscosity between 2 and 6 cP.

5.3. Results for vegetable oil

The physical properties of straight vegetable oil are quite similar to those of biodiesel, except for the viscosity. Vegetable oil is therefore suitable to nearly isolate the effect of increased viscosity on the spray quality. Any influence of temperature on the atomization performance is consequently assumed to be caused by viscous effects.

In contrast to the biodiesel cases, preheating was required to achieve an acceptable degree of atomization. An evident relation between the spray and the oil temperature was hence already seen during the measurements in the experimental setup. This relation is further illustrated in Fig. 11, showing the NLA for the vegetable oil sprays at temperatures between 50 and 100 °C. It can be seen that the NLA is clearly reduced by increasing the temperature until it reaches a certain minimum value. This reduction indicates that ligaments appear less frequently as the primary breakup is enhanced at lower viscosities. The temperature at which the minimum NLA is reached depends on the pressure. The detected ligament area is reduced between 50 and 90 °C at a pressure of 10 bar, while at 30 bar it is redundant to preheat to temperatures

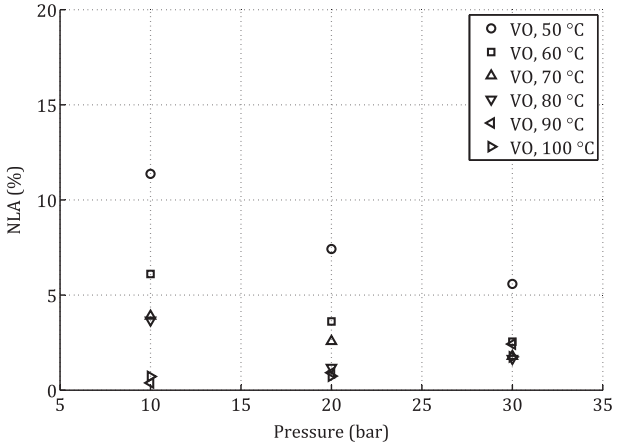

Fig. 11. Normalized ligament area as function of pressure for vegetable oil.

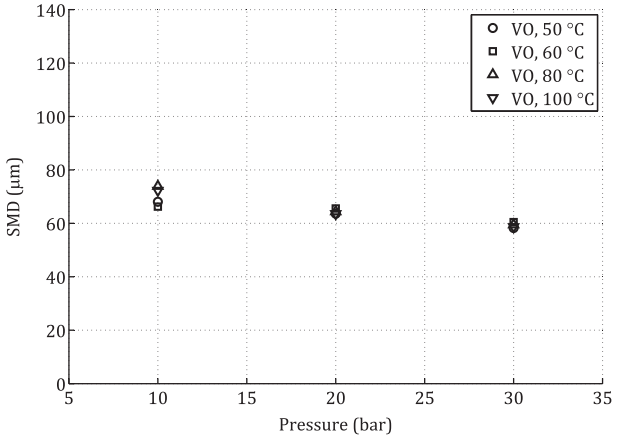

Fig. 13. SMD as function of pressure for vegetable oil.

above 60 °C. It can thus be concluded that the effect of temperature is more pronounced at lower pressures.

The minimum NLA that can be reached slightly increases towards higher pressures. Such a trend was also observed in the biodiesel results described previously (see Fig. 9) and can be attributed to secondary breakup. Here, it is important to note the similarity in viscosity of both liquids at these conditions, as can be seen in Fig. 7.

Since a significant portion of the spray volume is represented by ligaments at some of the investigated conditions, the mean ligament size is considered in addition to the NLA. In Fig. 12, the MLS is given as function of pressure for the temperatures at which the NLA exceeds 3%. A consistent trend is observed towards smaller ligaments with increasing pressure and temperature. The graph illustrates that the influence of the injection conditions is in fact stronger than suggested by the NLA data in Fig. 11. Raising pressure or temperature not only reduces the penetration depth of ligaments but also decreases their average size, thereby promoting the heat transfer to the spray in two different ways.

Fig. 13 presents the SMD of the droplets in the vegetable oil sprays at temperatures between 50 and 100 °C. Considering the strong influence of temperature on the primary breakup process, it is remarkable to see that such a clear dependency is not observed in the results for the mean droplet size. Variations with temperature are only noticed at a pressure of 10 bar, where the SMD fluctuates between 66 and 74 μm, though the relation between temperature and droplet size is inconsistent. Possibly, only the thin ligaments were disintegrated, while the thicker ones are still largely intact at this pressure. Since ligaments are not included in the SMD calculation, higher viscosity might lead to a lower droplet size in some cases. Increasing the pressure causes a slight reduction in SMD.

The mean droplet sizes shown in the figure are similar to those measured in the biodiesel cases, see Fig. 10. The results for vegetable oil in comparison to biodiesel therefore suggest that the droplets formed during primary atomization are not responsible for any major combustion issues. Instead, the problematic combustion behavior of a fuel with such a high viscosity is more likely caused by the tendency of ligaments to persist. As the breakup of ligaments is delayed or even prevented due to viscous dissipation, a high temperature or more atomization energy is required to restore the spray quality.

5.4. Results for glycerin

Regarding atomization, the physical properties of the glycerin are different from those of biodiesel in every aspect (see Table 1). It must therefore be kept in mind that the trends for glycerin may describe effects of surface tension and density next to viscosity. Considerable differences are also observed with respect to the vegetable oil properties, although the viscosities of both liquids are in the same range. In the following discussion of the results for glycerin, the differences with respect to the vegetable oil data are occasionally illustrated by referring to the spray images given as

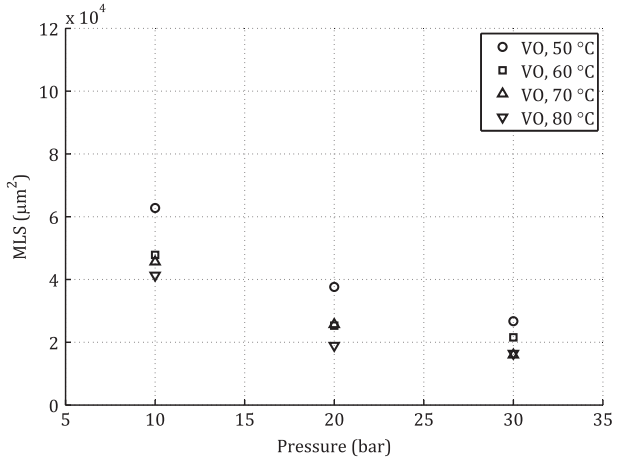

Fig. 12. Mean ligament size as function of pressure for vegetable oil.

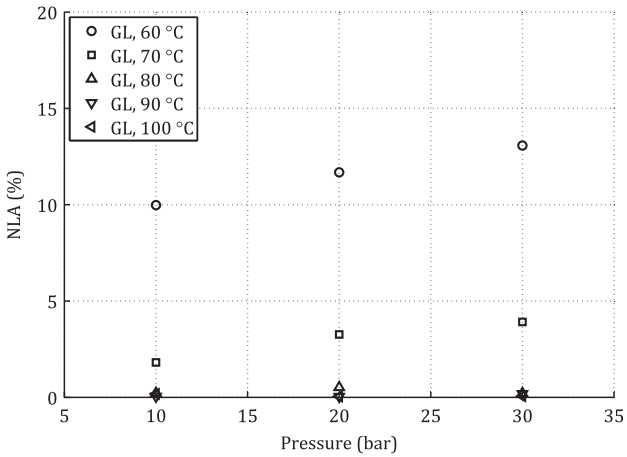

Fig. 14. Normalized ligament area as function of pressure for glycerin.

examples in Appendix C. In this appendix, glycerin sprays are compared to vegetable oil sprays at equal viscosity and injection pressure.

Measurements with glycerin were performed at temperatures starting from 60 °C to avoid capturing the liquid film that leaves the atomizer orifice. In Fig. 14, however, high NLA levels show that the primary breakup is still incomplete at temperatures under 80 °C. A typical image taken from the 10 bar glycerin spray at 60 °C is given in Fig. C.25. The snapshot of the glycerin spray is shown next to a representative image taken from the vegetable oil spray for the same pressure and viscosity. The ligaments visible in each image confirm the deterioration of the atomizer performance at such conditions. By studying all images captured from the two sprays in a qualitative manner, it is found that the sprays are quite similar regarding the frequency and size of the ligaments.

At high pressure, however, this similarity is not observed anymore. Compared to the vegetable oil spray, the ligaments in the glycerin spray at 30 bar are generally larger and besides seen more frequently. The difference in size is illustrated in Fig. C.26, where the two images show the largest ligament found in respectively the glycerin and the vegetable oil spray. This insight is also provided by considering the NLA data for both sprays. The upward trend of the NLA with pressure in Fig. 14 is indeed opposite to the trend seen in Fig. 11 for the vegetable oil spray. Since the viscosity is the same in these cases, the deviating trend for glycerin must be related to the combination of high surface tension and increased liquid density.

When the glycerin temperature is 80 °C or above, the primary breakup occurs upstream of the measurement location. Although the NLA in Fig. 14 is indeed expected to decrease due to reduced viscosity, the graph shows exceptionally low values at all pressures. This behavior is a consequence of the surface tension, which quickly forces the liquid elements into a spherical form once primary breakup has occurred. Since ligaments are distinguished from droplets based on their roundness, virtually all objects detected in the images are identified as droplets. The strong shape-preserving tendency also suppresses further breakup of the droplets. The slight increase in NLA with pressure, measured for biodiesel and vegetable oil at such low viscosities (see Figs. 9 and 11), is therefore not observed here. Manual inspection of the images confirm that secondary breakup does hardly occur. The difference in droplet shape between glycerin and vegetable oil sprays is visually illustrated by the images in Fig. C.27.

Fig. 15 shows that the average size of the ligaments detected in the glycerin sprays is decreased by raising the pressure. This trend agrees with the results for vegetable oil given in Fig. 12 and

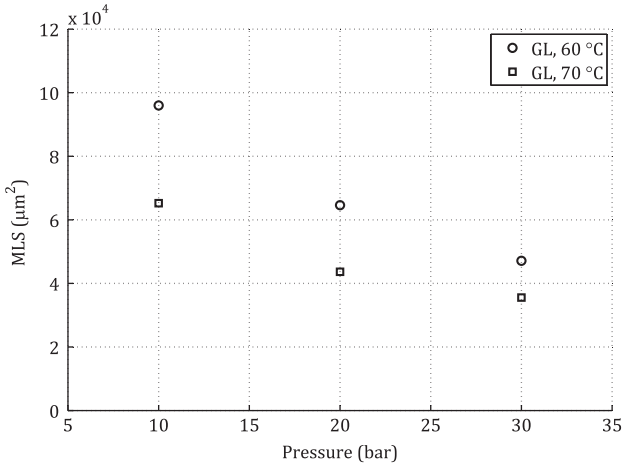

Fig. 15. Mean ligament size as function of pressure for glycerin.

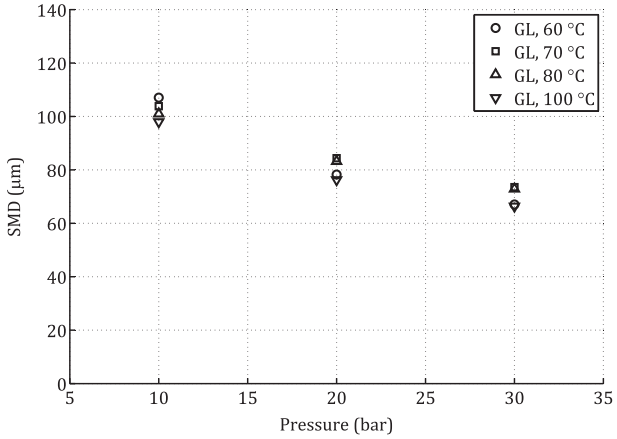

Fig. 16. SMD as function of pressure for glycerin.

confirms that the breakup of ligaments is improved when more atomization energy is transferred to the liquid.

The SMD of the sprays in the temperature range 60 to 100 °C is given in Fig. 16. A comparison with the data for biodiesel and vegetable oil in Figs. 10 and 13, respectively, indicates that the glycerin droplets are significantly larger at all conditions. The difference is highest at 10 bar, where the SMD of glycerin is 100–110 μm against 70–80 μm for the other two liquids. Even though the primary atomization is complete at 80 °C and above, such large droplets are not likely to evaporate fast enough in a conventional gas turbine combustor. The mean droplet size can be reduced by increasing the atomization energy via the pressure, but a pressure of 30 bar is needed to obtain similar SMD values as measured in the vegetable oil sprays at only 10 bar. Again, the SMD does not show a consistent relation with temperature. For this reason, the atomization quality at the sample location cannot be derived from the droplet data only.

5.5. Comparison with combustion experiments

The biodiesel and vegetable oil used in the present study have also been tested in the MMGT setup. This setup was recently employed to investigate the influence of viscosity on the burning performance of the two biofuels in a micro gas turbine [20]. Since the fuel spray was produced by the same atomizer in both studies, it is interesting to compare the results from the combustion experiments with the measured spray characteristics reported above.

In combustion tests with vegetable oil in idle mode, the exhaust gas contained a significant amount of unburned fuel in the form of blue smoke when the viscosity exceeded 9 cP. The smoke was assumed to be caused by incomplete evaporation of the fuel, creating fuel-rich zones in which the fuel is partly cracked instead of combusted. In such case, the poor breakup should be recognizable in the spray characteristics at such conditions. Given that the injection pressure during these tests was 13 bar and that the combustion chamber pressure was 2.0 to 2.5 bar, the pressure difference over the atomizer was approximately the same as in the 10 bar cases in the present study.

As mentioned in Section 5.3, the vegetable oil spray quality is most likely determined by the ligaments observed in the spray. Therefore, the viscosity limit that followed from the burning tests is to be compared with the NLA as function of viscosity, shown in Fig. 17 for a pressure of 10 bar. The figure indicates that the delay in primary breakup becomes visible in the images when the viscosity exceeds 7 cP. This turning point is in fairly good agreement

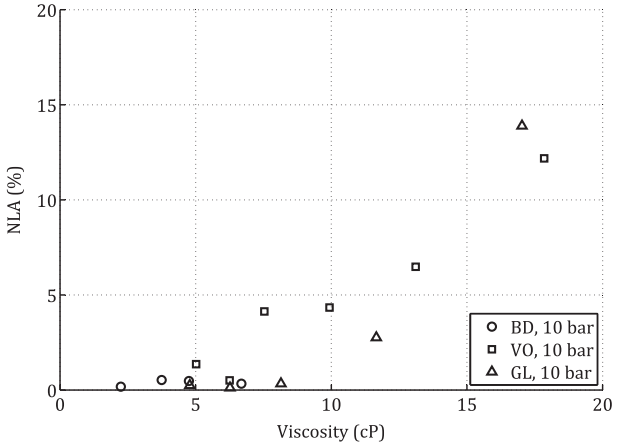

Fig. 17. Normalized ligament area as function of viscosity at a pressure of 10 bar.

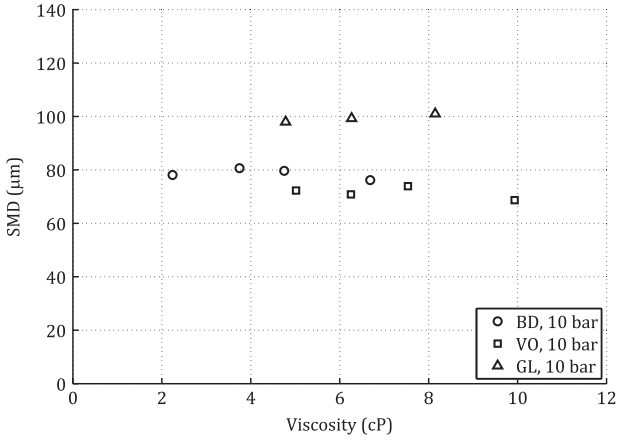

Fig. 19. SMD as function of viscosity at a pressure of 10 bar.

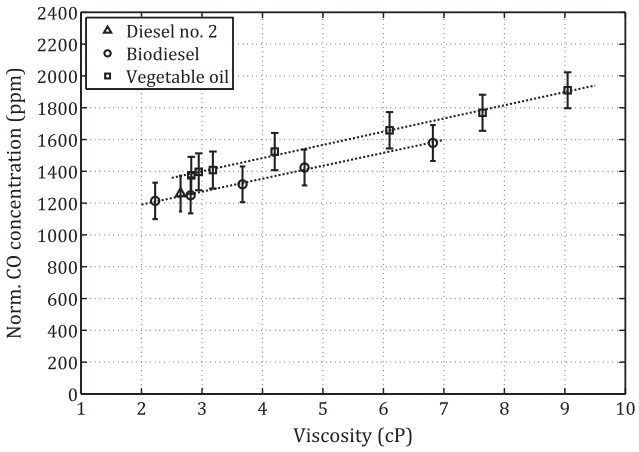

Fig. 18. CO emissions at 15 vol.% O_2 as function of viscosity for No. 2 diesel, biodiesel and vegetable oil.

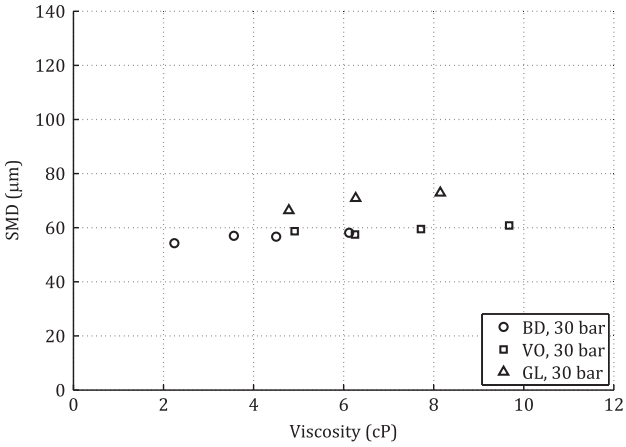

Fig. 20. SMD as function of viscosity at a pressure of 30 bar.

with the combustion tests. The small difference of 2 cP can be related to a few uncertain factors that could have promoted the breakup in the combustion chamber. Firstly, the flame might have been located slightly downstream of the sample location, which would give ligaments more time to break up before entering the flame. Secondly, the atomizer cooling flow and swirling air flow enveloping the spray may have caused additional instabilities. According to Lefebvre and Ballal [9], also the higher air density in the combustor can lead to a shorter breakup length. For these reasons, it is well possible that the adverse effects of ligament formation were slightly suppressed in the combustor with respect to the current measurements in the spray rig.

Another result from the combustion tests is the relation between viscosity and CO emissions as shown in Fig. 18. For both biodiesel and vegetable oil injected at 12 to 13 bar, the CO concentration in the exhaust gas was found to increase linearly with viscosity in the range 2 to 9 cP. Fig. 19 reports the SMD of the investigated 10 bar sprays with viscosities up to 10 cP. The graph shows that the assumed relation between viscosity and droplet size in this range cannot be confirmed. In fact, the SMD is quite insensitive to viscosity, which suggests that the decrease in CO emissions is primarily related to the breakup length of the spray, see Fig. 17. Fig. 20 shows a slight increase in SMD with viscosity for the 30 bar sprays, but this effect is small compared to the influence of pressure.

In Figs. 19 and 20, it is seen that the SMDs for glycerin are relatively large with respect to those for biodiesel and vegetable oil. These graphs therefore show that liquids with high density and surface tension are atomized less efficiently, irrespective of the viscosity. The influence of density with respect to surface tension has not been investigated in the present study. However, it is noted that the density is usually considered as the least significant among the three liquid properties affecting the spray structure [39]. The relative variation in density between the tested liquids is besides considerably lower than the relative difference in surface tension, see Table 1. Therefore, it can be expected that the surface tension plays a more important role here by inhibiting the formation of additional surface area.

5.6. Implications for pyrolysis oil combustion

The results obtained in the present study can used to estimate the technical feasibility of burning pure pyrolysis oil in a gas turbine by employing pressure-swirl atomization. As outlined in the introduction, fine atomization is a critical aspect considering the adverse properties of this biofuel compared to conventional fuels. The experiments with biodiesel, vegetable oil and glycerin are therefore valuable for predicting the atomizer performance with pyrolysis oil by comparing the liquid properties, among which the surface tension and viscosity are most important.

The surface tension of pyrolysis oil at room temperature can be as high as 40 mN/m, but mostly varies between 29 and

36 mN/m [2,37,40–44]. These values are higher than those of conventional gas turbine fuels at room temperature, such as No. 2 diesel (28 mN/m). However, the difference becomes small if the pyrolysis oil is preheated. Values between 24 and 32 mN/m have been reported for pyrolysis oil at a temperature of 80 °C [40,42–44], which are very similar to those of biodiesel and vegetable oil in this study (see Table 1). The surface tension should therefore not form a significant obstacle for the atomization of preheated pyrolysis oil.

An evaluation of the viscosity, however, makes clear that pressure-swirl atomizers are generally unsuitable for the application of pyrolysis oil in gas turbines. The viscosity limit obtained from the combustion experiments in the MMGT setup is 9 cP. The high sensitivity of the pressure-swirl method to this property also follows from the present atomization study. Although the viscosity of pyrolysis oil is not well-defined since it depends on the feedstock, the production process and the oil's age, the typical values reported in the literature vary between 5 and 30 cP for a temperature of 80 °C [1,2,45,46]. Higher temperatures should be avoided because of the chemical instability of this biofuel [45]. It is hence likely that pyrolysis oil, even when preheated, will exceed the range for which a pressure-swirl atomizer produces sprays of sufficient quality.

In the best case scenario, when the viscosity is under 7 cP, the pyrolysis oil spray has a short breakup length as indicated by Fig. 17 and an SMD similar to those measured for biodiesel and vegetable oil. Still, this is by no means a guarantee for an acceptable combustion quality. The composition of pyrolysis oil is very different from that of biodiesel and vegetable oil, in such a way that the evaporation and combustion processes are slower. Also, various pyrolysis oil fractions tend to form char inside the droplets during evaporation. These solid droplet residues burn very slowly and may damage the combustor or turbine blades, depending on their temperature history [47,48]. To minimize the evaporation time and the formation of char, pyrolysis oil combustion requires a finer spray than typically sufficient for light fossil fuels. Earlier studies have shown that the char formation is significantly reduced by lowering the SMD down to approximately 30 μm [10,44]. The graph in Fig. 20 illustrates that, even at a pressure of 30 bar, the tested atomizer is uncapable of delivering sprays for which the SMD is below 50 μm. It is therefore expected that the combustion of pure pyrolysis oil in the MMGT setup is not feasible when using a pressure-swirl atomizer. To greatly improve the atomization performance and make the breakup length less sensitive to viscosity, it is strongly recommended to use a more effective type of atomizer. Recent studies discussed in Section 1 indicate that certain twin-fluid atomizers are promising alternatives.

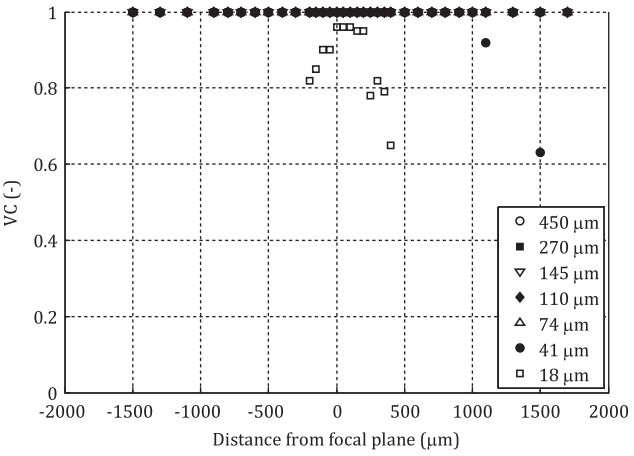

Fig. A.22. VC as function of the distance from the focal plane.

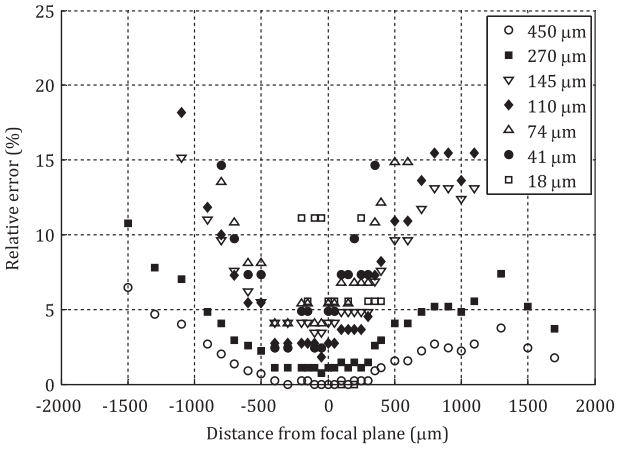

Fig. A.23. Relative measurement error as function of the distance from the focal plane.

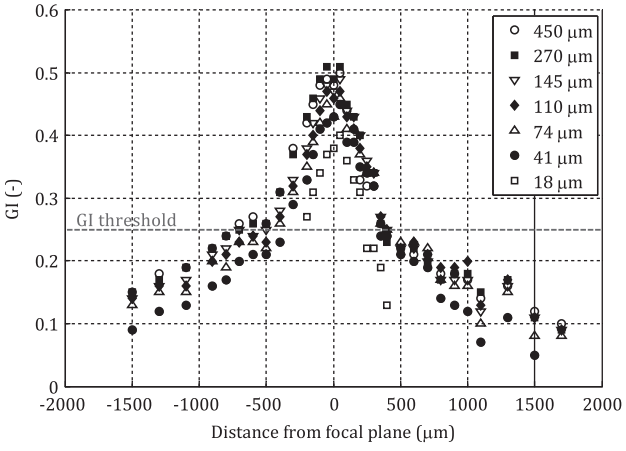

Fig. A.21. GI as function of the distance from the focal plane.

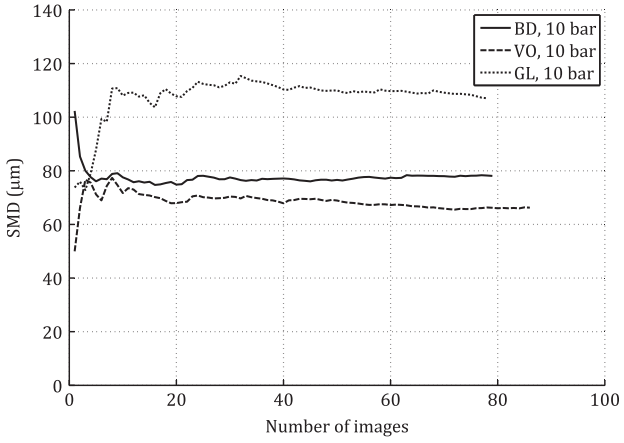

Fig. B.24. SMD as function of the number of images in the data set for sprays at 60 °C.

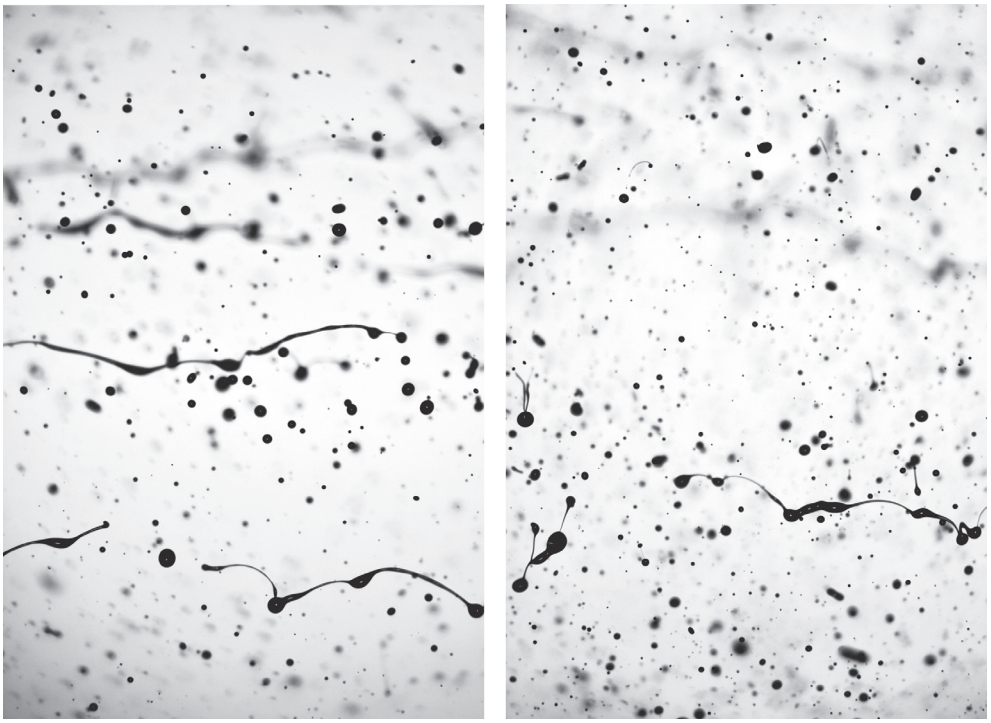

(a) GL, 10 bar, 60 °C (b) VO, 10 bar, 50 °C

Fig. C.25. Example images of a glycerin spray (a) and vegetable oil spray (b) at low pressure and low temperature. The viscosity of both liquids is about 17 cP.

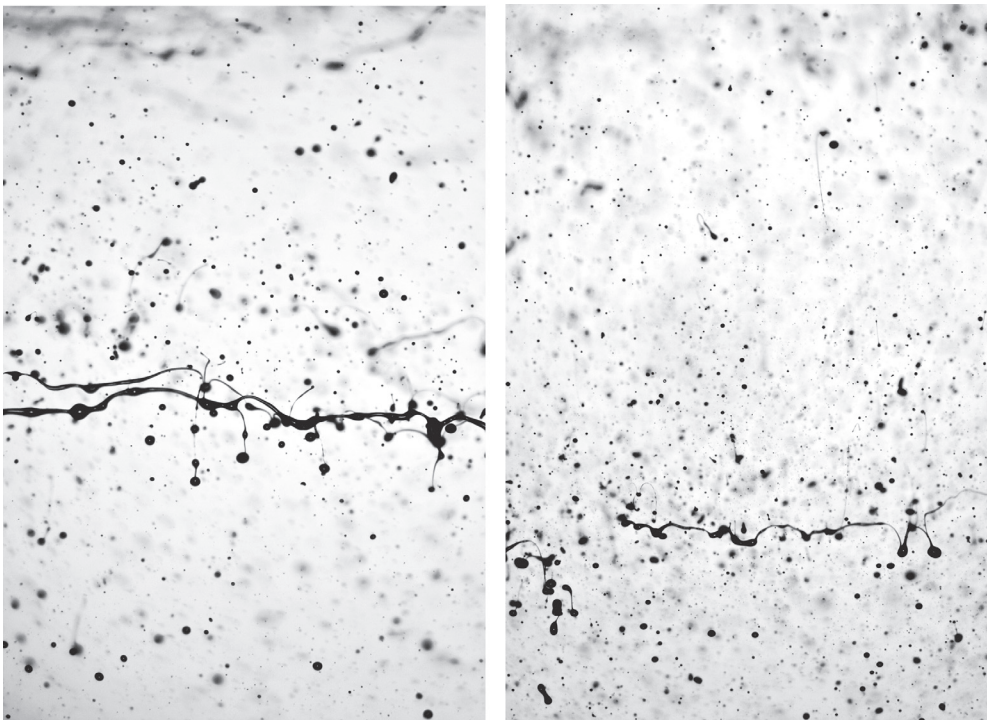

(a) GL, 30 bar, 60 °C (b) VO, 30 bar, 50 °C

Fig. C.26. Example images of a glycerin spray (a) and vegetable oil spray (b) at high pressure and low temperature. The viscosity of both liquids is about 17 cP.

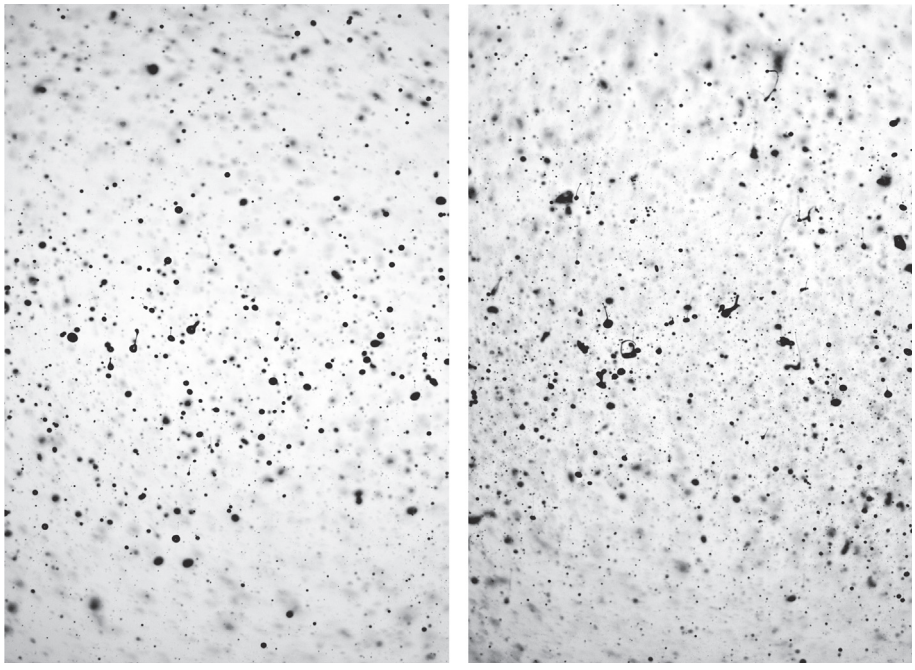

(a) GL, 30 bar, 100 °C (b) VO, 30 bar, 100 °C

Fig. C.27. Example images of a glycerin spray (a) and vegetable oil spray (b) at high pressure and high temperature. The viscosity of both liquids is 4.8 cP.

6. Conclusions

The atomization of biodiesel, vegetable oil and glycerin has been studied in an atmospheric spray rig by using digital imaging (PDIA). Images were captured 18 mm downstream of the atomizer to investigate the spray structure in the primary breakup region. The images were processed to automatically determine the size of ligaments and droplets. The sprays were produced by a pressure-swirl atomizer that originates from the MMGT setup. Various injection conditions have been tested to investigate the influence of mainly viscosity on the spray characteristics and to assess the overall performance of the atomizer. The spray measurements have been compared to combustion experiments with biodiesel and vegetable oil in the micro gas turbine at similar injection conditions.

The results show that the primary breakup process rapidly deteriorates when the viscosity is increased. A higher viscosity increases the breakup length, which becomes visible at the measurement location in the form of ligaments. This effect leads to an unacceptable spray quality once the viscosity slightly exceeds the typical range for conventional gas turbine fuels. Only biodiesel was atomized without problems at all test conditions, which covered viscosities in the range 2–6 cP. In case of vegetable oil, a decrease in atomizer performance was measured for viscosities above 7 cP. This value is in reasonably good agreement with the upper limit of 9 cP found during combustion experiments in the MMGT setup. In the images of the glycerin sprays, ligaments started to appear at viscosities between 8 and 12 cP.

Regarding the SMD of the sprays, no significant effect of viscosity is observed in the range 2–10 cP. The decrease in combustion efficiency measured over this viscosity range therefore cannot be explained by the average drop sizes in the primary breakup region. Instead, the delayed breakup of ligaments is considered as the main issue when burning viscous fuels. The results from the glycerin sprays indicate that a high surface tension causes an appreciable increase in SMD.

The current findings show that pressure-swirl atomization is unsuitable for the application of pure pyrolysis oil in an unmodified gas turbine engine, mainly due to the formation of persistent ligaments at increased viscosity.

Acknowledgment

The authors would like to thank the Province of Overijssel for sponsoring this work as part of the BE2.O program.

Appendix A. Results from the depth of field analysis

Figs. A.21, A.22, A.23

Appendix B. Convergence of the mean droplet size

Fig. B.24

Appendix C. Comparison between glycerin and vegetable oil sprays

Figs. C.25, C.26, C.27

References

[1] Mohan D, Pittman CU, Steele PH. Pyrolysis of wood/biomass for bio-oil: a critical review. Energy Fuels 2006;20(3):848–89. http://dx.doi.org/10.1021/Ef0502397.

[2] López Juste G, Salvá Monfort JJ. Preliminary test on combustion of wood derived fast pyrolysis oils in a gas turbine combustor. Biomass Bioenergy 2000;19(2):119–28. http://dx.doi.org/10.1016/S0961-9534(00)00023-4.

[3] Strenziok R, Hansen U, Künstner H. Combustion of bio-oil in a gas turbine. In: Bridgwater AV, editor. Progress in thermochemical biomass conversion. Oxford, UK: Blackwell Science Ltd.; 2001. p. 1452–8 [chapter 119]. http://dx.doi.org/10.1002/9780470694954.ch119.

[4] Razbin V, Coyle I. Emission Tests on ORENDA's OGT 2500 gas turbine. Tech. Rep. CETC-O-ACT-04-043-1 (CF), CANMET Energy Technology Centre, Ottawa, Canada; 2004.

[5] Lupandin V, Thamburaj R, Nikolayev A. Test results of the OGT2500 gas turbine engine running on alternative fuels: BioOil, ethanol, BioDiesel and crude oil. In: ASME Turbo Expo 2005. Reno, NV, USA: ASME; 2005. p. 421–6. http://dx.doi.org/10.1115/GT2005-68488.

[6] Tzanetakis T, Farra N, Moloodi S, Lamont W, McGrath A, Thomson MJ. Spray combustion characteristics and gaseous emissions of a wood derived fast pyrolysis liquid-ethanol blend in a pilot stabilized swirl burner. Energy Fuels 2010;24(10):5331–48. http://dx.doi.org/10.1021/Ef100670z.

[7] Beran M. Pyrolysis oil application in opra gas turbines 2011. <http://www.bioliquids-chp.eu/news.php?aid=16>.

[8] Beran M, Axelsson LU. Development and experimental investigation of a tubular combustor for pyrolysis oil burning. J Eng Gas Turbines Power 2015;137(3):31508. http://dx.doi.org/10.1115/1.4028450.

[9] Lefebvre AH, Ballal DR. Gas turbine combustion: alternative fuels and emissions. CRC Press; 2010. ISBN: 9781420086041.

[10] van Rossum G, Guell BM, Ramachandran RPB, Seshan K, Lefferts L, Van Swaaij WPM, et al. Evaporation of pyrolysis oil: product distribution and residue char analysis. Aiche J 2010;56(8):2200–10. http://dx.doi.org/10.1002/Aic.12126.

[11] Chhiti Y, Salvador S, Commandre JM, Broust F. Thermal decomposition of bio-oil: focus on the products yields under different pyrolysis conditions. Fuel 2012;102:274–81. http://dx.doi.org/10.1016/j.fuel.2012.06.098.

[12] Krumdieck SP, Daily JW. Evaluating the feasibility of biomass pyrolysis oil for spray combustion applications. Combust Sci Technol 1998;134(1–6):351–65. http://dx.doi.org/10.1080/00102209808924140.

[13] Garcia-Perez M, Chaala A, Kretschmer D, De Champlain A, Huges P, Roy C. Spray characterization of a softwood bark vacuum pyrolysis oil. In: Bridgwater A, Boocock D, editors. Proceedings of the science in thermal and chemical biomass conversion. Victoria, BC, Canada; 2004. p. 1468–79.

[14] Crayford AP, Bowen PJ, Kay PJ, Laget H. Comparison of gas-oil and bio-oil spray performance for use in a gas turbine. In: ASME Turbo Expo 2010. Glasgow, UK: ASME; 2010. p. 659–67. http://dx.doi.org/10.1115/GT2010-23485.

[15] Panchasara HV, Agrawal AK. Characteristics of preheated bio-oil sprays produced by an air-blast injector. In: ASME Turbo Expo 2010: power for land, sea, and air. American Society of Mechanical Engineers; 2010. p. 619–29. http://dx.doi.org/10.1115/GT2010-23397.

[16] Gañán Calvo AM. Enhanced liquid atomization: from flow-focusing to flow-blurring. Appl Phys Lett 2005;86(21):214101. http://dx.doi.org/10.1063/1.1931057.

[17] Simmons BM, Agrawal AK. Spray characteristics of a flow-blurring atomizer. Atom Sprays 2010;20(9). http://dx.doi.org/10.1615/AtomizSpr.v20.i9.60.

[18] Simmons BM, Agrawal AK. Flow and dropsize measurements in glycerol spray flames. In: 50th AIAA aerospace sciences meeting including the new horizons forum and aerospace exposition. Aerospace sciences meetings; American Institute of Aeronautics and Astronautics; 2012. http://dx.doi.org/10.2514/6.2012-523.

[19] Simmons BM, Agrawal AK. Drop size and velocity measurements in bio-oil sprays produced by the flow-blurring injector. In: ASME 2011 Turbo Expo: turbine technical conference and exposition. American Society of Mechanical Engineers; 2011. p. 701–10. http://dx.doi.org/10.1115/GT2011-46832.

[20] Sallevelt JLHP, Gudde JEP, Pozarlik AK, Brem G. The impact of spray quality on the combustion of a viscous biofuel in a micro gas turbine. Appl Energy 2014;132:575–85. http://dx.doi.org/10.1016/j.apenergy.2014.07.030.

[21] Kashdan JT, Shrimpton JS, Whybrew A. A digital image analysis technique for quantitative characterisation of high-speed sprays. Opt Lasers Eng 2007;45(1):106–15. http://dx.doi.org/10.1016/j.optlaseng.2006.03.006.

[22] Castrejón-García R, Castrejón-Pita JR, Martin GD, Hutchings IM. The shadowgraph imaging technique and its modern application to fluid jets and drops. Revista Mexicana Física 2011;57(3):266–75.

[23] Lecuona A, Sosa PA, Rodriguez PA, Zequeira RI. Volumetric characterization of dispersed two-phase flows by digital image analysis. Measure Sci Technol 2000;11(8):1152.

[24] Gepperth S, Guildenbecher D, Koch R, Bauer HJ. Pre-filming primary atomization: experiments and modeling. In: 23rd Annual conference on liquid atomization and spray systems; 2010. p. 1–9.

[25] Lad N, Aroussi A, Muhamad Said MFM. Droplet size measurement for liquid spray using digital image analysis technique. J Appl Sci 2011;11(11):1966–72. http://dx.doi.org/10.3923/jas.2011.1966.1972.

[26] Avulapati MM, Ravikrishna RV. An experimental study on effervescent atomization of bio-oil fuels. Atom Sprays 2012;22(8):663–85. http://dx.doi.org/10.1615/AtomizSpr.2012006482.

[27] Kourmatzis A, Pham PX, Masri AR. Air assisted atomization and spray density characterization of ethanol and a range of biodiesels. Fuel 2013;108:758–70. http://dx.doi.org/10.1016/j.fuel.2013.01.069.

[28] Gepperth S, Koch R, Bauer HJ. Analysis and comparison of primary droplet characteristics in the near field of a prefilming airblast atomizer. In: ASME Turbo Expo 2013. San Antonio, Texas, USA: ASME; 2013. V01AT04A002. ISBN: 978-0-7918-5510-2. http://dx.doi.org/10.1115/GT2013-94033.

[29] Castanet G, Dunand P, Caballina O, Lemoine F. High-speed shadow imagery to characterize the size and velocity of the secondary droplets produced by drop impacts onto a heated surface. Exp Fluids 2013;54(3):1–17. http://dx.doi.org/10.1007/s00348-013-1489-3.

[30] Canny J. A computational approach to edge detection. IEEE Trans Pattern Anal Machine Intell 1986;8(6):679–98.

[31] Lee SY, Kim YD. Sizing of spray particles using image processing technique. KSME Int J 2004;18(6):879–94. http://dx.doi.org/10.1007/BF02990860.

[32] Patterson HS, Cawood W. The determination of size distribution in smokes. Trans Faraday Society 1936;32:1084–8.

[33] Gasturbinen DG4M-1 und DG4M Beschreibung und Nutzung; 1978.

[34] Baroutian S, Aroua MK, Raman AAA, Sulaiman NMN. Density of palm oil-based methyl ester. J Chem Eng Data 2008;53(3):877–80. http://dx.doi.org/10.1021/je700682d.

[35] Esteban B, Riba JR, Baquero G, Puig R, Rius A. Characterization of the surface tension of vegetable oils to be used as fuel in diesel engines. Fuel 2012;102:231–8. http://dx.doi.org/10.1016/j.fuel.2012.07.042.

[36] Glycerine Producers' Association. Physical properties of glycerine and its solutions. Glycerine Producers' Association; 1963.

[37] Shaddix CR, Hardesty DR. Combustion properties of biomass flash pyrolysis oils: final project report. Tech. Rep. SAND99-8238, Sandia National Labs, Livermore, CA, USA; 1999.

[38] Ashgriz N, editor. Handbook of atomization and sprays: theory and applications. Springer; 2011.

[39] Lefebvre AH. Atomization and sprays. CRC; 1988.

[40] Boucher M, Chaala A, Roy C. Bio-oils obtained by vacuum pyrolysis of softwood bark as a liquid fuel for gas turbines. Part I: Properties of bio-oil and its blends with methanol and a pyrolytic aqueous phase. Biomass Bioenergy 2000;19(5):337–50. http://dx.doi.org/10.1016/S0961-9534(00)00043-X.

[41] Chiaramonti D, Oasmaa A, Solantausta Y. Power generation using fast pyrolysis liquids from biomass. Renew Sustain Energy Rev 2007;11(6):1056–86. http://dx.doi.org/10.1016/j.rser.2005.07.008.

[42] Garcìa-Pérez M, Chaala A, Pakdel H, Kretschmer D, Roy C. Vacuum pyrolysis of softwood and hardwood biomass. J Anal Appl Pyrolysis 2007;78(1):104–16. http://dx.doi.org/10.1016/j.jaap.2006.05.003.

[43] Tzanetakis T, Ashgriz N, James DF, Thomson MJ. Liquid fuel properties of a hardwood-derived bio-oil fraction. Energy Fuels 2008;22(4):2725–33. http://dx.doi.org/10.1021/ef7007425.

[44] Wissmiller D, Brown RC, Meyer TR. Pyrolysis oil combustion characteristics and exhaust emissions in a swirl-stabilized flame. Ph.D. thesis, Iowa State University; 2009.

[45] Boucher ME, Chaala A, Pakdel H, Roy C. Bio-oils obtained by vacuum pyrolysis of softwood bark as a liquid fuel for gas turbines. Part II: Stability and ageing of bio-oil and its blends with methanol and a pyrolytic aqueous phase. Biomass Bioenergy 2000;19(5):351–61. http://dx.doi.org/10.1016/S0961-9534(00)00044-1.

[46] Oasmaa A, Peacocke C, Gust S, Meier D, McLellan R. Norms and standards for pyrolysis liquids. End-user requirements and specifications. Energy Fuels 2005;19(5):2155–63. http://dx.doi.org/10.1021/Ef040094o.

[47] D'Alessio J, Lazzaro M, Massoli P, Moccia V. Thermo-optical investigation of burning biomass pyrolysis oil droplets. Symp (Int) Combust 1998;27(2):1915–22. http://dx.doi.org/10.1016/S0082-0784(98)80035-0.

[48] Garcia-Perez M, Lappas P, Hughes P, Dell L, Chaala A, Kretschmer D, et al. Evaporation and combustion characteristics of biomass vacuum pyrolysis oils. IFRF Combust J 2006;200601:1–27.